PCCP

Accepted Manuscript

ROYAL SOCIETY OF CHEMISTRY

www.rsc.org/pccp

Physical Chemistry Chemical Physics
CREATED USING THE RSC LaTeX PCCP ARTICLE TEMPLATE – SEE www.rsc.org/electronicfiles FOR DETAILS
ARTICLE TYPE www. rsc.org/xxxxxx | XXXXXXXX

Enhanced thermoelectric efficiency in ferromagnetic silicene nanoribbons terminated with hydrogen atoms

K. Zberecki[1], R. Swirkowicz[1], M. Wierzbicki[1], J. Barnaś[2]

Received Xth XXXXXXXXXX 20XX, Accepted Xth XXXXXXXXX 20XX
First published on the web Xth XXXXXXXXXX 200X
DOI: 10.1039/b000000x

Using ab-initio methods we calculate thermoelectric and spin thermoelectric properties of silicene nanoribbons with bare, mono-hydrogenated and di-hydrogenated edges. Asymmetric structures, in which one edge is either bare or di-hydrogenated while the other edge is mono-hydrogenated (0H-1H and 2H-1H nanoribbons) have ferromagnetic ground state and display remarkable conventional and spin thermoelectric properties. Strong enhancement of the thermoelectric efficiency, both conventional and spin ones, results from a very specific band structure of such nanoribbons, where one spin channel is blocked due to an energy gap while the other spin channel is highly conducting. In turn, 0H-2H and 2H-2H nanoribbons (with one edge being either bare or di-hydrogenated and the other edge being di-hydrogenated) are antiferromagnetic in the ground state. Accordingly, the corresponding spin channels are equivalent, and only conventional thermoelectric effects can occur in these nanoribbons.

1 Introduction

Thermoelectric phenomena in various nanostructures are currently of great interest due to the possibility of converting dissipated heat to electrical energy at nanoscale. Some nanostructures can exhibit relatively high thermoelectric efficiency, being thus suitable candidates for applications in nanoelectronics devices as elements of power generators or cooling systems. It is already well known that quantum confinement and Coulomb blockade in nanoscale junctions with quantum dots and molecules can lead to a considerable enhancement of the heat to current conversion efficiency [1–3].

Very recently, new two-dimensional materials like graphene and silicene – especially one-dimensional graphene nanoribbons (GNRs) and silicene nanoribbons (SiNRs) – have been attracting a great interest due to their unique properties [4–8]. Though thermopower S of pristine graphene is not very high (S close to 100 μV/K has been reported [9]) its value can be considerably enhanced in GNRs, especially in nanostructures consisting of nanoribbons of various types. Indeed, in a properly designed nanoribbon with alternating zigzag and armchair sections, thermoelectric figure of merit exceeding unity at room temperature has been found [10]. The efficiency can be also enhanced by randomly distributed hydrogen vacancies in almost completely hydrogenated GNRs [11]. Furthermore, structural defects, especially in the form of anti-dots, also appear a promising way to enhance thermoelectric efficiency [12–14]. Indeed, giant spin related thermoelectric phenomena have been predicted for ferromagnetic zigzag graphene nanoribbons (zGNRs) with antidots [14].

In nanoscale systems, in which two spin channels are not equivalent and not mixed by spin-flip processes, spin related thermoelectric phenomena can be observed in addition to the conventional thermoelectric effects. These spin related phenomena result from interplay of spin, charge and heat transport [15]. For instance, in ferromagnetic nanostructures one can observe the spin Seebeck effect, which is a spin analog of the well known Seebeck effect and is associated with thermal generation of spin voltage. This phenomenon was observed in thin films [16,17] and also in magnetic tunnel junctions [18,19].

Since silicon plays a crucial role in the present-day electronics, integration of silicene – a two-dimensional hexagonal lattice of silicon atoms – into nanoelectronics seems to be more promising than that of graphene. Therefore, understanding of physical properties of silicene is currently of great interest. Electronic structure of silicene is similar to that of graphene, i.e. silicene is a semimetal with low-energy states at the Fermi level described by the Dirac model [20]. However, due to the buckled atomic structure it is possible to open an energy gap with electric field [21,22]. Quite recently, silicene nanoribbons have been fabricated [23], and their properties have been widely studied theoretically by ab-initio methods [24–29]. Silicene nanoribbons of zigzag type, similarly to graphene ones, can exhibit magnetic ordering of edge moments. Ab-initio calculations show that the lowest-energy state of nanoribbons with edges symmetrically terminated with atomic hydrogen is antiferromagnetic, where magnetic moments at one edge are

[1] *Faculty of Physics, Warsaw University of Technology, ul. Koszykowa 75, 00-662 Warsaw, Poland*
[2] *Faculty of Physics, Adam Mickiewicz University, ul. Umultowska 85, 61-614 Poznań, Poland*
and Institute of Molecular Physics, Polish Academy of Sciences, Smoluchowskiego 17, 60-179 Poznań, Poland

antiparalell to those at the other edge[27–29]. Such a nanoribbon behaves like a semiconductor, with a relatively wide energy gap. However, in the presence of external magnetic field, a ferromagnetic state with all moments ordered in parallel can be stabilized[28]. The system behaves then as a metallic ferromagnet with constant transmission in the vicinity of the Fermi level[28]. On the other hand, the one-side ferromagnetic state, with magnetic moments localized only along one edge, can be induced in the presence of densely distributed impurities (like boron or nitrogen) at the other edge[31,39]. The nanoribbon behaves then as a spin gapless semiconductor, where one spin channel is blocked for conduction due to an energy gap while the second spin channel is gapless.

Experimental and theoretical studies have shown that electronic and magnetic properties of zigzag silicene nanoribbons (zSiNRs) are strongly influenced by the presence of hydrogen[29,32]. Based on the density-functional-theory (DFT) calculations it has been found that at low hydrogen concentration, zSiNRs with edges terminated with atomic hydrogen are stable, whereas at ambient conditions nanoribbons with dihydrogenated edges can appear[29]. It has been also predicted that hydrogen-terminated zSiNRs subject to in-plane electrical field behave like a half-metallic ferromagnet with spin polarization up to 99%[33].

In the present paper we study the effects of edge hydrogenation on electronic transport and thermoelectric properties of zSiNRs. The considerations clearly show that nanoribbons with asymmetrically terminated edges, where one edge is mono-hydrogenated while the other edge is either bare or dihydrogenated, exhibit stable ferromagnetic state and also pronounced thermoelectric properties – both conventional and spin ones. The predicted thermoelectric efficiency is exceptionally high and results from the very specific band structure, with the gaps corresponding to the two spin channels remarkably shifted in energy. Accordingly, one spin channel can be conductive in a certain region of chemical potential, whereas the second channel is then blocked for transport and thus gives rise to a high thermopower. Due to their remarkable electronic and thermoelectric properties, ferromagnetic zSiNRs with hydrogenated edges have a huge potential for various applications in nanoelectronic and nanothermoelectric devices.

The paper is organized as follows. In section 2 we describe the computational method used to calculate band structure and transmission function. We also provide there a general description of thermoelectric properties. Numerical results on electric and thermoelectric properties are presented and discussed in section 3. Final conclusions are in section 4.

2 Theoretical description

2.1 Transmission

To investigate electronic transport through zSiNRs, we used the ab-initio approach within the the DFT Siesta code[34,35]. Numerical calculations were performed for nanoribbons containing N=6 zigzag chains. In order to analyze the influence of hydrogen termination at the nanoribbon edges on the magnetic, transport and thermoelectric properties, we will consider the following four different situations: (i) 1H-0H systems, in which one edge of zSiNRs is terminated with atomic hydrogen, whereas the dangling bonds appear at the other edge; (ii) 1H-2H structures, where one edge is mono-hydrogenated and the other one is dihydrogenated; (iii) 2H-0H nanoribbons with one edge dihydrogenated and the other being free of hydrogen; and (iv) 2H-2H nanoribbons, with both edges being dihydrogenated. The simple structure, 1H-1H, with both edges terminated with atomic hydrogen was discussed earlier[28], so this situation will be omitted in the present paper.

All the structures under consideration were optimized until atomic forces converged to 0.02 eV/A. Furthermore, the atomic double-polarized basis (DZP) was used and the grid mesh cutoff was set equal to 200 Ry. Apart from this, the generalized gradient approximation (GGA) with Perdrew-Burke-Ernzerhof parameterization was applied to the exchange-correlation part of the total energy functional[36].

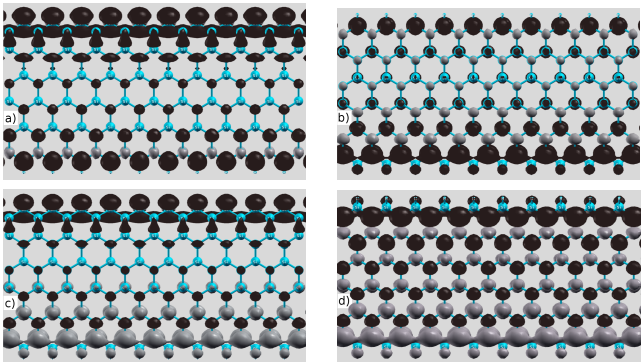

Fig. 1 (Color online) Spin density distribution in the ferromagnetic (FM) (a,b) and antiferromagnetic (AFM) (c,d) ground states, calculated for zSiNR of 1H-0H (a), 1H-2H (b), 2H-0H (c) and 2H-2H (d) types. Black and grey dots represent magnetic moments of opposite orientations.

Numerical calculations show that the nanoribbons under consideration exhibit magnetic ordering in the ground state. The corresponding spin density distribution across the nanoribbons is presented in Fig. 1. The ground state of zSiNRs with 1H-0H and 1H-2H edges is ferromagnetic (FM), with the corresponding energy lower than that of antiferro-

magnetic (AFM) configuration by 0.01 eV and 0.02 eV, respectively. On the other hand, the most stable configuration of the nanoribbons of 2H-0H and 2H-2H types is antiferromagnetic, with magnetic moments at one edge being opposite to those at the other edge (Figs 1c,d). Energy of the AFM state is smaller than the energy of the corresponding FM state, respectively by 0.06 eV for 2H-0H and 0.01 eV for 2H-2H nanoribbons. Other possible configurations, eg. one-sided ferromagnetic or nonmagnetic ones, have considerably higher energy.

The spin-resolved energy-dependent transmission function $T_\sigma(E)$ through the nanoribbons was determined within the non-equilibrium Green function method (NGF) as implemented in the Transiesta code [35]. Having determined the transmission $T_\sigma(E)$, one can calculate transport properties (including also thermoelectric ones) of the nanoribbons, as described below.

2.2 Thermoelectricity

When the spin channels are mixed in the nanoribbon on a distance comparable to the system length, no spin related thermoelectric properties can be observed and only conventional thermoelectric phenomena occur. We will consider first this limit. In the linear response regime, the electric I and heat I_Q currents flowing through the system from left to right, when the electrical potential and temperature of the left electrode are higher by δV and δT, respectively, can be written in the matrix form as [28,37,38]

$$\begin{pmatrix} I \\ I_Q \end{pmatrix} = \begin{pmatrix} e^2 L_0^+ & \frac{e}{T} L_1^+ \\ e L_1^+ & \frac{1}{T} L_2^+ \end{pmatrix} \begin{pmatrix} \delta V \\ \delta T \end{pmatrix}, \qquad (1)$$

where e is the electron charge, while $L_n^+ = L_{n\uparrow} + L_{n\downarrow}$, with $L_{n\sigma} = -\frac{1}{h}\int dE\, T_\sigma(E)\,(E-\mu)^n \frac{\partial f}{\partial E}$ for $n = 0,1,2$. Here, T_σ(E) is the spin-dependent transmission function (described above) for the system and $f(E-\mu)$ is the Fermi-Dirac distribution function corresponding to the chemical potential μ and temperature T. The electrical conductance G (for $\delta T = 0$) is given as $G = e^2(L_{0\uparrow} + L_{0\downarrow}) \equiv G_\uparrow + G_\downarrow$, whereas the electronic contribution to the thermal conductance, κ_e, defined by heat current at $I = 0$, is equal to

$$\kappa_e = \frac{1}{T}\left(L_2^+ - \frac{L_1^{+2}}{L_0^+}\right). \qquad (2)$$

The thermopower, defined as $S = -\delta V/\delta T$ for $I = 0$, is given by the formula

$$S = -\frac{L_1^+}{|e|TL_0^+}. \qquad (3)$$

In turn, the thermoelectric efficiency of the system is described by the figure of merit ZT defined as

$$ZT = \frac{S^2 GT}{\kappa}, \qquad (4)$$

where κ corresponds to the total thermal conductance due to electrons and phonons, $\kappa = \kappa_e + \kappa_{ph}$.

Situation may change when the spin channels are either not mixed in the nanoribbon or they are mixed on a scale much longer than the system's size. The spin effects in thermoelectricity become then important and to describe them one needs to introduce spin voltage δV_s and also spin current I_s. The formula (1) can be then generalized to the following one:

$$\begin{pmatrix} I \\ I_s \\ I_Q \end{pmatrix} = \begin{pmatrix} e^2 L_0^+ & e^2 L_0^- & \frac{e}{T} L_1^+ \\ e^2 L_0^- & e^2 L_0^+ & \frac{e}{T} L_1^- \\ e L_1^+ & e L_1^- & \frac{1}{T} L_2^+ \end{pmatrix} \begin{pmatrix} \delta V \\ \delta V_s \\ \delta T \end{pmatrix}, \qquad (5)$$

where the spin current I_s is normalized to $\hbar/2e$, while $L_n^- = L_{n\uparrow} - L_{n\downarrow}$ and L_n^+ is defined as above. The electrical conductance (for $\delta V_s = 0$ and $\delta T = 0$) of the system is then given by the formula $G = e^2(L_{0\uparrow} + L_{0\downarrow}) \equiv G_\uparrow + G_\downarrow$, while the spin conductance (for $\delta V = 0$ and $\delta T = 0$) is given by $G_s = e^2(L_{0\uparrow} - L_{0\downarrow}) = G_\uparrow - G_\downarrow$. In turn, the electronic contribution to the thermal conductance, κ_e, defined by the heat current at $I = 0$ and $I_s = 0$, is given by [39]

$$\kappa_e = \frac{1}{T}\sum_\sigma \left(L_{2\sigma} - \frac{L_{1\sigma}^2}{L_{0\sigma}}\right). \qquad (6)$$

The conventional (charge) thermopower can be defined as $S_c = -\delta V/\delta T$ at $I = 0$ and $I_s = 0$, while the spin thermopower as $S_s = -\delta V_s/\delta T$ also for $I = 0$ and $I_s = 0$. Thus, the thermopowers can be written in the form [39]

$$S_c = -\frac{1}{2|e|T}(L_{1\uparrow}/L_{0\uparrow} + L_{1\downarrow}/L_{0\downarrow}) \equiv \frac{1}{2}(S_{c\uparrow} + S_{c\downarrow}),$$
$$S_s = -\frac{1}{2|e|T}(L_{1\uparrow}/L_{0\uparrow} - L_{1\downarrow}/L_{0\downarrow}) \equiv \frac{1}{2}(S_{c\uparrow} - S_{c\downarrow}). \qquad (7)$$

To describe the conventional (charge) and spin thermoelectric efficiency, one can introduce the corresponding figures of merit, defined as

$$ZT_c = \frac{S_c^2 GT}{\kappa}, \;\; ZT_s = \frac{S_s^2 |G_s| T}{\kappa}. \qquad (8)$$

Alternatively, one can define the conventional thermopower as $S_c = -(\delta V/\delta T)$ for $I = 0$ and $\delta V_s = 0$, and the spin thermopower as $S_s = -(\delta V_s/\delta T)$ for $I_s = 0$ and $\delta V = 0$ [40]. The thermopowers are then given by the formulas $S_c = -L_1^+/(|e|TL_0^+)$ and $S_s = -L_1^-/(|e|TL_0^+)$. Similarly, the heat conductance can be defined by the heat current at $I = 0$ and $\delta V_s = 0$, and thus is given by Eq.(6). The two different definitions depend essentially on experimental conditions. In the following numerical calculations we will use the former definitions given by Eqs (6-8).

In the linear response regime, considered here, transport properties are determined by electronic states near the Fermi

level. In reality the chemical potential in nanoribbons (measured from the Fermi energy) can be easily varied near the Fermi level with an external gate voltage. Alternatively, the chemical potential can be moved down or up by p-type or n-type doping, which results in $\mu < 0$ and $\mu > 0$, respectively.

3 Ferromagnetic zSiNRs

In nanoribbons with FM ordering of the edge magnetic moments, the spin-up and spin-down channels are generally different. If the corresponding spin relaxation time is long enough, the spin thermoelectric effects become observable. Assuming this is the case, we consider spin-dependent transport and spin thermoelectric phenomena in zSiNRs of 1H-0H and 1H-2H types [41]. The limit of independent of spin transport, when only conventional thermoelectric effects can be observed, will be considered in the next section for systems with AFM ordering.

3.1 zSiNRs of 1H-0H type

Spin-polarized electronic bands as well as the spin-resolved transmission function, calculated for the ferromagnetic 1H-0H nanoribbon, are presented in Fig.2. This figure clearly shows,

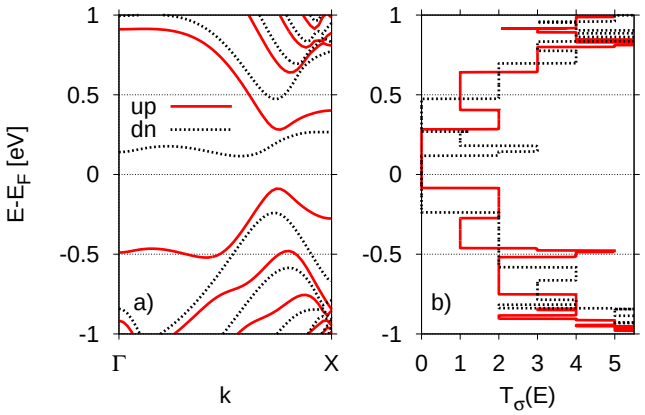

Fig. 2 (Color online) Spin-resolved band structure (a) and transmission function (b) calculated for zSiNR of 1H-0H type. The energy is measured with respect to the Fermi energy E_F of the corresponding pristine nanoribbon.

that the nanoribbon behaves like a ferromagnetic semiconductor with a spin-dependent energy gap in the vicinity of the Fermi level. When the energy E decreases below the Fermi energy E_F, then the first electronic states below the Fermi level correspond to the spin-up channel and are located in the spin-down gap. The situation is different for energies above E_F, where a narrow spin-down band is located in the spin-up gap, but close to the gap edge. With a further increase in energy, another gap for spin-minority (spin-down) electrons opens in the spin-up band. Thus, there is a spin dependent energy gap at the Fermi level, and one additional gap for spin-down electrons at higher energies. All these gaps are very well visible in the spin-resolved transmission function presented in Fig.2b. Moreover, these gaps strongly influence spin-dependent transport properties, including also thermoelectric phenomena, as shown below for the temperature of 90 K which has been chosen in order to have correspondence with the results obtained earlier[28].

Spin resolved electrical conductance is presented in Fig. 3a as a function of the chemical potential measured from the Fermi energy E_F. Due to the presence of spin-dependent energy gaps, there are regions of chemical potential, where one of the spin channels is blocked for transport while the other one is conductive. This leads to large spin polarization P of the charge current, defined as $P = \frac{G_\uparrow - G_\downarrow}{G_\uparrow + G_\downarrow} \times 100\%$. Note that for negative μ, just below the Fermi level, only the spin-up channel in conductive, whereas in a wide region of positive μ this channel is blocked and the spin-down channel dominates transport. Accordingly, the current polarization achieves $\pm 100\%$, and changes sign in the vicinity of the Fermi level (corresponding to μ=0). It is also interesting to note, that the electrical conductance exhibits a considerably high maximum just above the Fermi level, which appears due to the presence of a relatively flat band corresponding to the spin-down electrons. Thus, relatively small changes in the chemical potential allow to achieve quite good conduction, with almost total, $\pm 100\%$, spin polarization. The situation is totally different in pristine zSiNRs symmetrically terminated with atomic hydrogen, which exhibit AFM ordering with a relatively wide energy gap. However, in the presence of external magnetic field, such nanoribbons behave like a metallic ferromagnet with both spin channels being conductive[28].

Thermal conductance due to electrons, κ_e, is presented in Fig. 3b as a function of the chemical potential μ. Similarly to the electric conductance, the thermal conductance is strongly suppressed in the energy gap and remarkably increases near the gap edges. This increase, however, is smaller than in zSiNRs symmetrically terminated with atomic hydrogen, as only one spin channel, corresponding either to spin-up or to spin-down electrons, can support heat current in the vicinity of the gap edges. The phonon heat conductance, shown in the inset to Fig.3d, was calculated using the 4- Nearest-Neighbor-Force Constant (4NNFC) model. The corresponding parameters of the model were determined from fitting of the phonon spectrum to that obtained from ab-initio approach for 2D silicene. As shown in the inset to Fig.3d, this conductance grows monotonously with increasing temperature.

Since the transmission through the system is strongly spin-

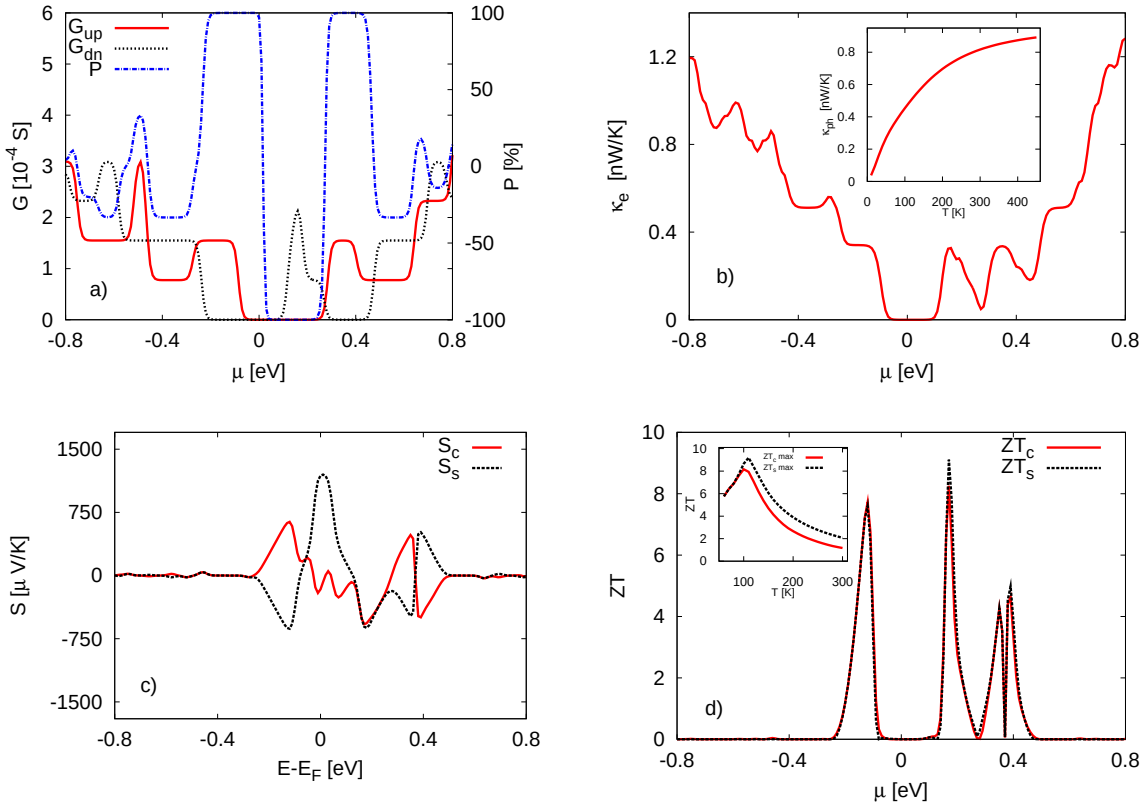

Fig. 3 (Color online) Spin-resolved electric conductance G_σ (G_{up} for spin-up and G_{dn} for spin-down electrons) and the corresponding spin polarization P (a); electronic term in the thermal conductance, κ_e (b); charge, S_c, and spin, S_s, thermopowers (c); and charge, ZT_c, and spin, ZT_s, figures of merit (d); calculated for the zSiNR of 1H-0H type and $T = 90$ K. The inset in (b) shows temperature dependence of the phonon contribution to the heat conductance, while the inset in (d) shows the temperature dependence of the maxima in ZT_c and ZT_s corresponding to the respective peaks at negative μ.

dependent, one can expect considerable spin effects in thermopower. The conventional S_c and spin S_s thermopowers are presented in Fig.3c as a function of chemical potential. Indeed, a huge value of S_s, close to 1.4 mV/K, is obtained in the vicinity of the Fermi energy (corresponding to $\mu = 0$). Then, S_s rapidly decreases to zero with increasing $|\mu|$, changes sign, and its magnitude achieves values close to -0.7 mV/K for certain narrow regions of the chemical potential. For positive μ, S_s changes sign once more and achieves a local maximum of ≈ 0.7 mV/K. For, larger values of $|\mu|$, when the chemical potential is well inside the electron bands and far from the gaps, the thermopower drops to small values, which are close to zero. The conventional thermopower S_c is less remarkable, though for certain regions of μ it also takes values close to 0.7 mV/K. High values of S_s/S_c are related to the presence of spin-dependent energy gaps in the spectrum, and especially to the very sharp transmission changes near the gap edges. For small negative chemical potentials, transport can be supported by spin-up holes as the spin-down channel is non-active due to the energy gap in this channel. Then, the rapid decrease in $T_\uparrow$ near E_F generates a high positive contribution to $S_\uparrow$. The situation is different just above the Fermi level, where the spin-down channel becomes conductive and the rapid increase in $T_\downarrow$ gives rise to a high negative contribution to $S_\downarrow$. Accordingly, the thermopowers $S_\uparrow$ and $S_\downarrow$, corresponding to the two spin channels, have opposite signs in the region close to μ=0, and therefore S_c is small, while S_s achieves the main maximum. When $|\mu|$ increases further, both $S_\uparrow$ and $S_\downarrow$ decrease and become equal to zero when flat parts of $T_\uparrow$ or $T_\downarrow$ are achieved. For higher values of negative μ, the main contribution comes then from the spin-down channel and corresponds to a rapid decrease in $T_\downarrow$ at the edge of the gap in this spin channel. Both S_c and S_s have then opposite signs. Behavior of the thermopowers for positive μ is then slightly different due to the additional gap in the spin-down channel as described above. This leads to additional positive local maximum in S_s and local minimum

in S_c around $\mu = 0.4$ eV, which appear close to the upper edge of the additional gap in the spin-down channel. Lower edge of this gap also leads to some features in the thermopowers as clearly seen in Fig.3c.

Consider now the thermoelectric efficiency described by the figures of merit ZT_c and ZT_s. Both ZT_c and ZT_s are presented in Fig.3d as a function of the chemical potential μ. Thermoelectric efficiency was determined taking into account the total heat conductance. Variation of both conventional ZT_c and spin ZT_s figures of merit with the chemical potential reveals two high peaks located in the vicinity of μ=0; one for negative and another one for positive μ. Apart from this, there are two additional peaks of lower intensity in both ZT_c and ZT_s, which appear for higher values of positive chemical potential. Temperature dependence of the maxima in ZT_c and ZT_s corresponding to the respective peaks for negative μ is shown in the inset to Fig.3d. From this figure follows that at room temperature both ZT_c and ZT_s are significantly smaller than in the low temperature regime.

The thermoelectric efficiency calculated here for 1H-0H zSiNRs is very remarkable, despite the total heat conductance is relatively high. Note that nanoribbons symmetrically terminated with atomic hydrogen exhibit much smaller thermoelectric efficiency[28]. This huge enhancement of the figures of merit comes mainly from the high power factors $S_c^2 G$ and $S_s^2 G_s$. Furthermore, S_c and S_s are strongly enhanced for $\mu < 0$ and $\mu > 0$ corresponding to the edges of energy gaps in the spin-down ($\mu < 0$) and spin-up ($\mu > 0$) channels. Additionally, the electrical conductance $G_\uparrow$ for $\mu < 0$ and $G_\downarrow$ for $\mu > 0$ is relatively high as the appropriate channel is conductive. Both power factors are thus enhanced, accordingly. Note, that the efficiency ZT_s shows no central peak, though the thermopower S_s has a maximum for $\mu \approx 0$. However, both spin channels are blocked in this region due to the energy gap in the spin-up and spin-down channels. High efficiency can be observed only in situation when one spin channel is blocked, while the second one is well conductive. It is worth of note, that similar enhancement of the thermoelectric efficiency was found in ferromagnetic graphene nanoribbons with structural defects in the form of antidots[14].

3.2 2H-1H ferromagnetic nanoribbons

Consider now the nanoribbons of 1H-2H type, where one edge is mono-hydrogenated while the other edge is dihydrogenated. The lowest-energy state of such nanoribbons is ferromagnetic, and the corresponding band structure is shown in Fig. 4a. In turn, Fig. 4b presents the spin-resolved transmission function. As follows from the band structure, the system is a semiconductor with wide gaps at the Fermi level for both spin-up and spin-down channels. These gaps, however, are shifted in energy, so the true energy gap at the Fermi level is rather narrow, despite the gaps for individual spin channels are relatively wide, much wider than in the case of 1H-0H nanoribbons analyzed above. However, there is now additional gap for spin-up channel (negative μ) and also for spin-down channel (positive μ). Interestingly, the relatively flat spin-down band above the Fermi energy is located almost in the middle of the spin-up gap at the Fermi level. Thus, the band structure in transmission is slightly reacher than in the case of 1H-0H nanoribbons studied above, as there is one additional gap. This specific form of the transmission function makes the corresponding variation of the thermoelectric parameters with the chemical potential more complex, as discussed below.

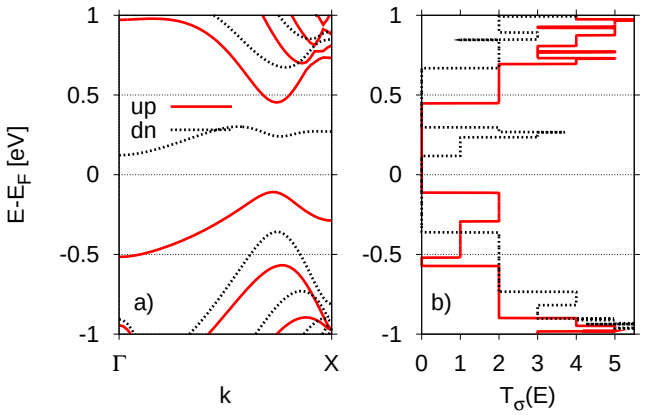

Fig. 4 (Color online) Spin-resolved band structure (a) and transmission function (b) calculated for zSiNR of 1H-2H type. The energy is measured with respect to the Fermi energy E_F of the corresponding pristine nanoribbon.

Chemical potential dependence of the key transport and thermoelectric parameters is shown in Fig.5. Similarly as in case of 1H-0H nanoribbons, the energy gaps are strongly spin dependent. Thus, there are regions of chemical potential where one spin channel is blocked for transport while the other channel is well conducting. As a result, one finds in these regions almost full spin polarization of charge current, as clearly visible in Fig.5 a. The spin polarization varies between $+100\%$ and -100%. Interestingly, a small change in the chemical potential in the vicinity of the Fermi level can results in a change of the current polarization from $P = -100\%$ to $P = +100\%$.

The results obtained for electronic contribution to the heat conductance are now interesting as there are two energy regions of suppressed κ_e, one around $\mu = 0$ and another one for higher positive values of μ. The low-temperature heat conductance in these regions is practically equal to zero. The two regions of suppressed electronic term in the thermal conductance correspond to the two true energy gaps in the electronic

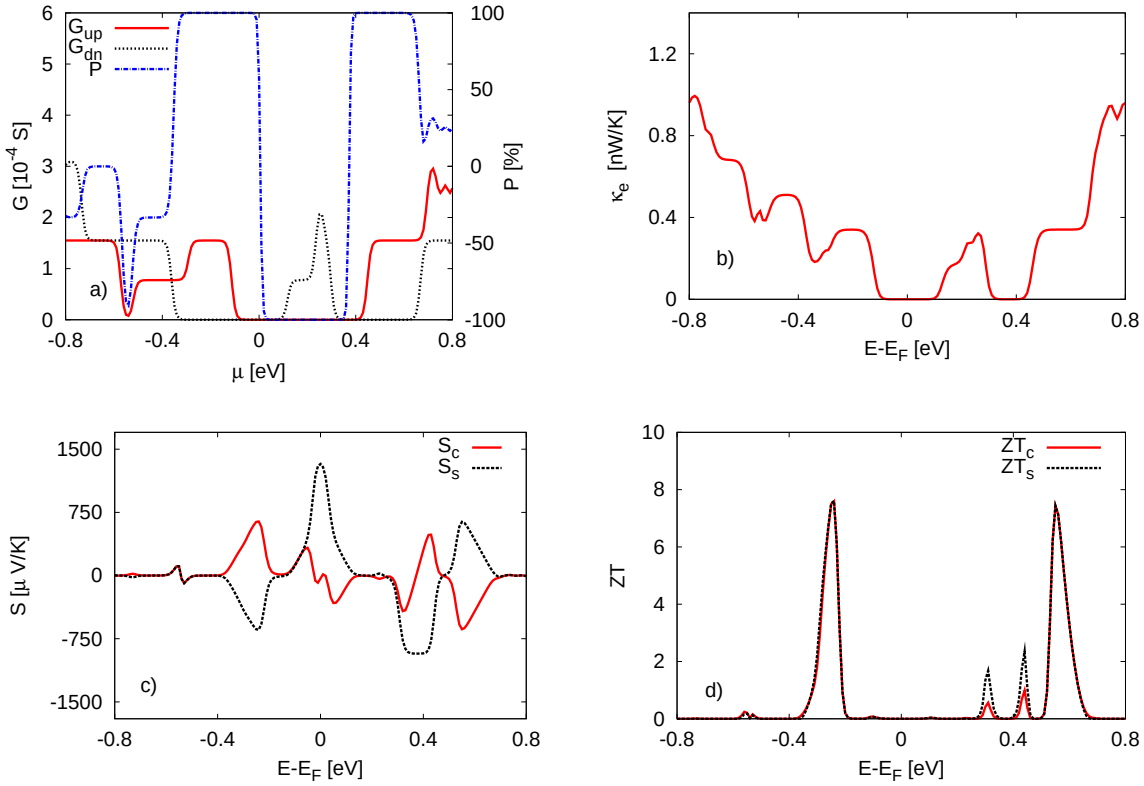

Fig. 5 (Color online) Spin-resolved electric conductance G_σ and the corresponding spin polarization P (a); electronic thermal conductance κ_e (b); charge, S_c, and spin, S_s, thermopower (c); charge, ZT_c, and spin, ZT_s, thermoelectric efficiency (d); calculated for zSiNR of 1H-2H type and $T = 90$ K.

spectrum – one gap for μ in the vicinity of the Fermi level and the other gap corresponding to the overlap of the main gap in the spin-up channel and the additional gap in the spin-down channel. The second additional gap (for negative μ) is a very narrow gap in one spin channel only, so it does not lead to suppression of κ_e and only contributes to the first dip seen in κ_e for negative μ.

The general behavior of the thermopower, both conventional S_c and spin S_s, is similar to that found in the case of in the case of 1H-0H nanoribbons considered above, with a huge central maximum in S_s near μ=0. However, the side maxima of $|S_s|$ and $|S_c|$ are shifted towards larger values of $|\mu|$. Additionally, the maximum in $|S_s|$ at positive chemical potential is broad and exceeds 0.8 mV/K. This maximum results mainly from the states near the left edge of the gap in the spin-down channel, which gives positive contribution to $S_\downarrow$. Electron states near the right edge of the spin-up gap give a negative contribution to $S_\uparrow$. As a result, a high value of $|S_s|$ can be achieved. The maximum is broad because the peaks in $S_\uparrow$ and $S_\downarrow$ are shifted with respect to each other. On the other hand, the conventional thermopower S_c , which corresponds to the sum of $S_\uparrow$ and $S_\downarrow$, is remarkably lower and changes sign in dependence on which quantity, $S_\uparrow$ or $S_\downarrow$, is predominant. Similar behavior can be observed in a close vicinity of μ=0, where S_s is remarkably enhanced while S_c is reduced due to the opposite signs of $S_\uparrow$ (positive) and $S_\downarrow$ (negative).

The conventional ZT_c and spin ZT_s figures of merit are presented in Fig. 5d as a function of the chemical potential. Both types of the thermoelectric efficiency are dominated by very high peaks appearing for negative and positive values of μ. However, due to relatively wide energy gaps, the peaks are located at higher values of $|\mu|$, especially in the region of positive chemical potential. The two peaks of lower intensity, which can be seen for positive μ, occur at the edges of the second energy gap in electronic spectrum (Fig. 4). The thermopower is then considerably enhanced, especially the spin thermopower, and the spin thermoelectric efficiency exceeds 2, accordingly. The results presented in this section clearly

demonstrate that details of the band structure in the vicinity of the Fermi energy strongly influence the thermoelectric efficiency. The gaps which are required to obtain high thermopower should be relatively narrow to give remarkable efficiency for small values of the chemical potential.

3.3 Antiferromagnetic nanoribbons

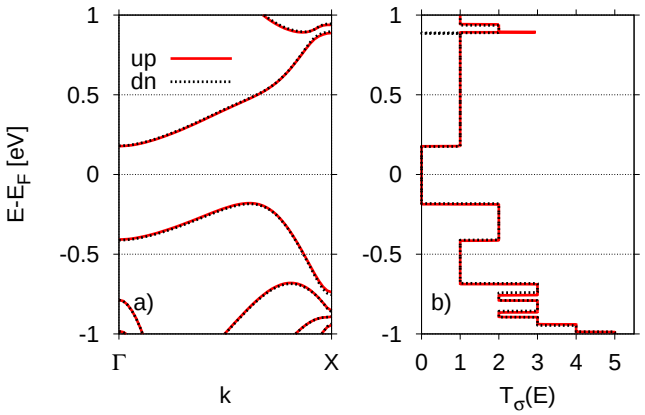

Fig. 6 (Color online) Spin-resolved band structure (a) and transmission function (b) calculated for zSiNR of 2H-2H type. The energy is measured with respect to the Fermi energy E_F of the corresponding pristine nanoribbon.

Finally, let us consider nanoribbons of 2H-2H and 2H-0H types, for which the most stable configuration is antiferromagnetic, ie. magnetic moments of the two edges are antiparallel. Nanoribbons of such types are semidonducting, with a wide energy gap near the Fermi level. Here we discuss only the 2H-2H type as the thermoelectric properties in both cases are very similar. The band structure and transmission function for the 2H-2H nanoribbon are presented in Fig. 6, whereas the electric and thermoelectric coefficients are shown in Fig.7. Since the bands are spin degenerate, only the conventional thermoelectric phenomena are relevant.

The presence of a wide energy gap can be well visible in both electric G (Fig. 7a) and electronic heat conductance κ_e (inset to Fig. 7a). The conductances increase considerably near the gap edges and are almost constant in a wide range of chemical potential due to constant transmission. The rapid decrease in transmission near the edge of the valence band, as well as the increase near the edge of conductance band, give rise to a huge thermopower exceeding 1.5 mV/K (Fig. 7b). The peaks in S appear at a distance of a few kT from the gap edges. However, despite of a remarkably high thermopower, the thermoelectric efficiency ZT is rather small (inset to Fig. 7b) since the electrical conductance is close to zero in the energy gap, which essentially reduces the power factor. Similar results are also obtained for the antiferromagnetic nanoribbon of 2H-0H type, though the thermoelectric efficiency in this case is lower. In general, the results are also similar to those obtained for zSiNRs symmetrically terminated with atomic hydrogen[28]. They are not so spectacular as for ferromagnetic nanoribbons, which are asymmetrically terminated with hydrogen (nanoribbons of 2H-1H and 1H-0H types discussed in the previous section). Accordingly, our analysis clearly shows that a relatively high thermoelectric efficiency can be achieved only in systems with two non-equivalent spin channels, in which an energy gap can appear in one spin channel whereas the second channel supports charge transport. Owing to this, such systems may have a great potential for applications in spintronic and thermoelectric nanodevices.

4 Summary and conclusions

We have considered thermoelectric properties of zSiNRs with bare, mono- and di-hydrogenated edges. Both symmetric as well as asymmetric cases have been analyzed. In the former case both edges are equivalent and are either mono-or di-hydrogenated. In the later case, in turn, the hydrogenation degree of one edge is different from that of the other edge. The asymmetrically terminated nanoribbons of 1H-0H and 2H-1H types exhibit ferromagnetic ground state, i.e magnetic moments at the two edges are parallel. Such nanoribbons reveal spin thermoelectric effects in addition to the conventional ones. Moreover, due to the specific band structure both spin and conventional thermoelectric efficiency are remarkably enhanced.

In turn, ground-state configuration in the nanoribbons of 2H-2H and 2H-0H types is antiferromagnetic, i.e. spin moments at one edge are opposite to those at the other edge. Accordingly, both spin channels are equivalent and only conventional thermoelectric effects are observable.

5 Acknowledgments

This work was supported by the National Science Center in Poland as the Project No. DEC-2012/04/A/ST3/00372. Numerical calculations were performed at the Interdisciplinary Centre for Mathematical and Computational Modelling (ICM) at Warsaw University and partly at SPINLAB computing facility at Adam Mickiewicz University.

References

1 R. Venkatasubramanian, E. Siivola, T. Colpitts, B. O'Quinn, Nature 413, 597 (2001).

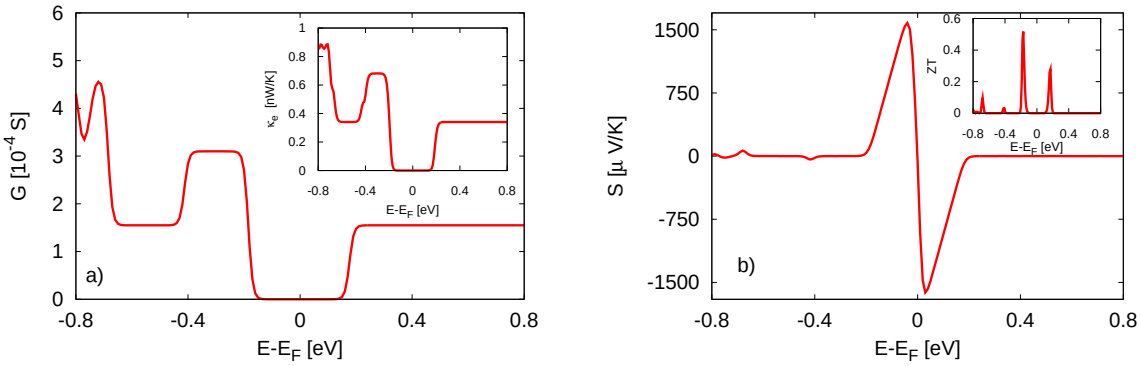

Fig. 7 (Color online) Electric conductance per spin channel (a), electronic thermal conductance κ_e (inset to a), thermopower S (b) and thermoelectric efficiency ZT (inset to b) calculated for zSiNR of 2H-2H type, T=90 K

2 A. I. Hochbaum, R. Chen, R.D. Delgado, W. Liang, E.C. Garnett, M. Najarian, A. Majumdar, P. Yang, Nature 451, 163 (2008).

3 T.C. Harman, P.J. Taylor, M.P. Walsh, B.E. LaForge, Science 297, 2229 (2002).

4 H. Haugen, D.Huertas-Hernando and A. Brataas, Phys. Rev. B77, 115406 (2008).

5 H.B. Heersche, P. Jarillo-Herrero, J.B. Oestinga, L.M. Vandersypen and A.F. Morpurgo, Nature 446,56 (2007).

6 B. Aufray, A. Kara, S. Vizzini, H. Oughaddou, C. Leandri, B. Ealet, G. Le Lay, Appl. Phys. Lett. 96, 183102 (2010).

7 P. D. Padova, C. Quaresima, B. Olivieri, P. Perfetti, and G. Le. Lay, Appl. Phys. Lett. 98, 081909 (2011).

8 P. Vogt, P. De Padova, C. Quaresima, J. Avila, E.Frantzeskakis, M.C. Asensio, A. Resta, B. Ealet, and G. Le Lay, Phys. Rev. Lett. 108, 155501 (2012).

9 Y.M. Zuev, W.Chang and P. Kim, Phys. Rev. Lett. 102, 096807 (2009)

10 F. Mazzamuto, V. Huang Nguyen, Y. Apertet, C. Caer, C. Chassat, J. Saint-Martin and P. Dollfus, Phys. Rev. B83, 235426 (2011)

11 Y. Ding and J. Ni, Appl. Phys. Lett. 95, 083115 (2009); W. Zhao, Z.X. Guo, J.X. Cao, and J.W. Ding, AIP Advances 1, 042135 (2011).

12 T.G. Pedersen, C. Flindt, J. Pedersen, N.A. Mortensen, A.P. Jauho, and K. Pedersen, Phys. Rev. Letters 100, 136804 (2008).

13 Y. Yan, Q.F. Liang, H. Zhao, C.Q. Wu, and B. Li, Phys. Letters A 376, 2425 (2012).

14 M. Wierzbicki, R. Swirkowicz and J. Barnaś, Phys. Rev. B 88, 235434 (2013).

15 K. Uchida, S. Takahashi, K. Harii, J. Ieda, W. Koshibae, K. Ando, S. Maekawa, E. Saitoh, Nature 455, 778 (2008).

16 K. Uchida, H. Adachi, T. An, T. Ota, M. Toda, B. Hillebrands, S. Maekawa, and E. Saitoh, Nature Mater.10, 737 (2011).

17 S.Y. Huang, W.G. Wang, S.F. Lee, J. Kwo, and C.L. Chien, Phys. Rev. Lett. 107, 216604 (2011).

18 M. Walter, J. Walowski, V. Zbarsky, M. Münzenberg, M. Schäfers, D. Ebke, G. Reiss, A. Thomas, P. Peretzki, M. Seibt, J.S. Moodera, M. Czerner, M. Bachmann, Ch. Heiliger, Nature Mat. 10, 742 (2011).

19 J.C. Le Breton, S. Sharma, H. Saito, S. Yuasa, and R. Jansen, Nature 475 , 82 (2011).

20 S. Cahangirov, M. Topsakal, S. Ciraci, Phys. Rev. B 81, 195120 (2010);

21 N.D.Drummond, V. Zolyomi and V.I. Fal'ko, Phys. Rev. B85, 075423 (2012).

22 Z. Ni, Q. Liu, K. Tang, J. Zeng, J. Zhou, R. Qin, Z. Gao, D. Yu and J. Lu, Nano Lett. 12, 113 (2012)

23 A. Kara, H. Enriquez, A. P. Seitsonen, L.C. Lew Yan Voon,, S. Vizzini, B. Aufray, H. Oughaddou, Surf. Sci. Rep. 67, 1-18 (2012).

24 J. Kang, F. Wu, J. Li, Appl. Phys. Lett. 100, 233122 (2012).

25 Ch. Xu, G. Luo, Q. Liu, J. Zheng, Z. Zhang, S. Nagase, Z. Gao, J. Lu, Nanoscale, 4, 3111 (2012).

26 Y. Liang, V. Wang, H. Mizuseki and Y. Kawazoe, J. Phys. Cond. Matter, 24, 455302 (2012).

27 L. Pan, H. J. Liu, X. J. Tan, H. Y. Lv, J. Shi, X. F. Tang, G. Zheng, Phys. Chem. Chem. Phys., 14, 13588-13593 (2012).

28 K. Zberecki, M. Wierzbicki, J. Barnaś, R. Swirkowicz, Phys. Rev B 88, 115404 (2013).

29 D.-Q. Fang, S.-L. Zhang, and H. Xu, RSC Advances 3, 24075 (2013).
30 Y. Ding, and Y. Wang, J. Phys. Chem. C, 117, 18266 (2013).
31 F. Zheng, C. Zhang, S. Yan and F. Li, J. Mater. Chem. C , 1, 2735 (2013).
32 M.E. Davila, A. Marele, P. DePadova, I. Montero, F. Hennies, A. Pietzasch, M.N. Shariati, J.M. Gomez-Rodriguez and G. Le Lay, Nanorechnology 23, 385703 (2012).
33 W. Wang, J. Zheng, Z. Ni, R. Fei, Q. Liu, R. Quhe, C. Xu, J. Zhou, Z. Gao and J. Lu, Nano 7, 1250037 (2012).
34 D. Sanchez-Portal, P. Ordejon, E. Artacho, J. M. Soler,Int. J. Quantum Chem. 65, 453 (1997).
35 M. Brandbyge, J.-L. Mozos, P. Ordejon, J. Taylor, K. Stokbro, Phys. Rev. B 65, 165401 (2002).
36 J.P. Perdew, K. Burke, and M. Ernzerhof. Phys. Rev. Lett., 77, 3865 (1996).
37 U. Sivan and Y. Imry, Phys. Rev. B **33**, 551 (1986).
38 C. D. Mahan, Many-Particle Physics (Plenum, New York, 2000).
39 R. Swirkowicz, M. Wierzbicki and J. Barnaś, Phys. Rev. B **80**, 195409 (2009).
40 Y. Dubi and M. Di Ventra, Phys. Rev. B **79** 081302 (2009).
41 B. Bishnoi and B. Ghosh, RSC Adv. 3, 26153 (2013).